

Mechanism of phase transitions and the electronic density of states in $(\text{La,Sm})\text{FeAsO}_{1-x}\text{F}_x$ from *ab initio* calculations

Peter V. Sushko,^{1,2,*} Alexander L. Shluger,² Masahiro Hirano,³ Hideo Hosono^{3*}

¹WPI-Advanced Institute for Materials Research, Tohoku University, Sendai, Japan

²Department of Physics & Astronomy, London Centre for Nanotechnology,
Materials Simulation Laboratory, University College London,
Gower Street, London WC1E 6BT, United Kingdom and

³Frontier Collaborative Research Center and Materials and Structures Laboratory,
Tokyo Institute of Technology, 4259 Nagatsuta, Midori-ku, Yokohama 226-8503, Japan

(Dated: February 10, 2022)

The structure and electronic density of states in layered $\text{LnFeAsO}_{1-x}\text{F}_x$ ($\text{Ln}=\text{La,Sm}$; $x=0.0, 0.125, 0.25$) are investigated using density functional theory. For the $x=0.0$ system we predict a complex potential energy surface, formed by close-lying single-well and double-well potentials, which gives rise to the tetragonal-to-orthorhombic structural transition, appearance of the magnetic order, and an anomaly in the specific heat capacity observed experimentally at temperatures below ~ 140 – 160 K. We propose a mechanism for these transitions and suggest that these phenomena are generic to all compounds containing FeAs layers. For $x > 0.0$ we demonstrate that transition temperatures to the superconducting state and their dependence on x correlate well with the calculated magnitude of the electronic density of states at the Fermi energy.

PACS numbers: 74.25.Jb, 61.50.Ah, 75.25.+z

The discovery of a new superconductor $\text{LaFeAsO}_{1-x}\text{F}_x$ with a high transition temperature ($T_c=26$ K) [1] has triggered a global search for other Fe-based alternatives to Cu-based superconductors, which have dominated the field since their discovery in 1986 [2]. Substituting As, Fe, and La for other pnictogens [3], transition metals [4] and lanthanides [5], respectively, applying external pressure [6], and optimizing the doping level have pushed the T_c to 54.5 K [7]. However, since then its value seems to have saturated. As doubts have been expressed that T_c can be raised any further [8], it became apparent that generic guiding principles for the T_c optimization need to be developed.

LaFeAsO is a member of the layered Fe-pnictogens, in which FeAs sheets are separated from each other by spacers such as layers of ionic oxide, e.g. LaO in LaFeAsO , [Fig. 1(a)] or metal atoms, e.g. Ba in BaFe_2As_2 [9]. In spite of the difference in the nature of the spacers, FeAs-based materials show surprising similarities in the temperature dependence of their structural parameters, anomalies in the electric resistance and specific heat capacity, and in their magnetic properties (e.g. [9, 10, 11, 12, 13]).

A series of theoretical and computational reports appeared recently describing the electronic properties, magnetic interactions, phonon structure, and the origin of the superconductivity in LaFeAsO and related compounds (e.g. [14, 15, 16, 17, 18, 19]). The aim of this work is twofold: (i) to develop a model for the phase transitions observed in FeAs-based materials and (ii) to investigate a correlation between electronic density of states at the Fermi energy and the experimentally observed values of the T_c and its dependence on the doping level.

The calculations were carried out using density func-

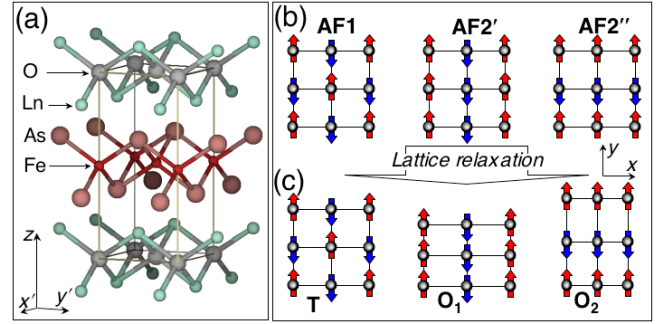


FIG. 1: (Color online) (a) Structure of 1×1 LnFeAsO ($\text{Ln} = \text{La, Sm}$) unit cell. (b) Schematics of several spin configurations within Fe layers shown for a $\sqrt{2} \times \sqrt{2}$ supercell. The circles show the positions of Fe atoms within the Fe layer. Here and below, up and down arrows indicate "up" and "down" spins, respectively. See text for details.

tional theory (DFT), the generalized gradient approximation functional PW91 [20] and the projected augmented waves method [21] implemented in the VASP code [22]. The plane-wave basis set cutoff was set to 600 eV. The supercells containing eight (1×1 , Fig. 1), 16 ($\sqrt{2} \times \sqrt{2}$), and 32 (2×2) atoms and Monkhorst-Pack grids of 252, 132, and 36 k -points, respectively, were used. For the analysis of the electronic structure, the charge-density was decomposed over atom-centered spherical harmonics.

In the first part of the paper we consider the relation between configurations of the spins associated with Fe $3d$ electrons and the lattice structure. Several ordered antiferromagnetic configurations in a $\sqrt{2} \times \sqrt{2}$ supercell are shown in Fig. 1(b). In AF1, the spins on the neighboring Fe atoms are antiparallel. In configurations AF2'

and AF2'' spins are parallel along y - and x -axes respectively; AF2' and AF2'' are equivalent in the case of the high-temperature tetragonal (T) phase.

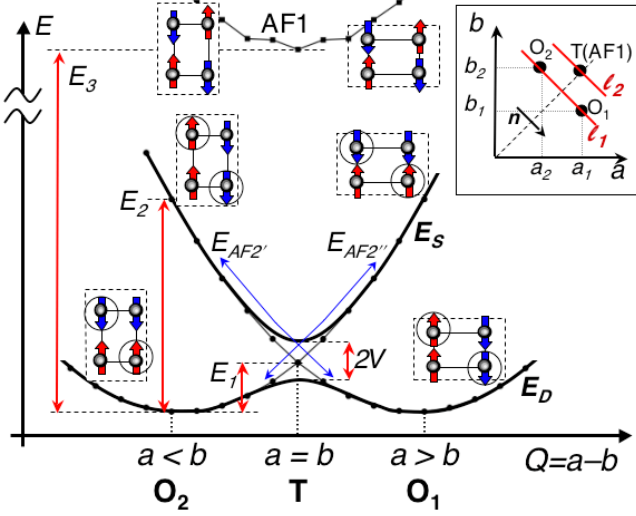


FIG. 2: Potential energy surfaces for the AF1 and AF2 configurations. Dots correspond to calculated energy values. Open circles indicate the spin pairs, which are different in \mathbf{O}_1 and \mathbf{O}_2 configurations.

After minimization of the total energies with respect to both the atomic positions and the lattice parameters, the AF1 configuration maintains the T structure (Table I). Configurations AF2' and AF2'' relax to two equivalent orthorhombic (O) structures \mathbf{O}_1 and \mathbf{O}_2 , in which the Fe 3d spins along the short Fe-Fe bonds are parallel and those along the long Fe-Fe bond are antiparallel [see Fig. 1(c)]. The lattice parameters a , b , and c for \mathbf{O}_1 and \mathbf{O}_2 relate as $a_1=b_2$, $b_1=a_2$, $c_1=c_2$, and $a_1>b_1$ (see also Fig. 2). The calculated values for the lattice parameters for the low-temperature O-phase agree with the experimental data to within 0.4 %. (Table I). The ferromagnetic configuration is considerably less stable than antiferromagnetic ones and is not considered here.

Integration of the AF2'' charge-density within LaO and FeAs layers shows that the layers are charged: $(\text{LaO})^{+\delta}(\text{FeAs})^{-\delta}$ with $\delta = 0.15 |e|$. Thus, one can consider LnFeAsO as a super-ionic compound, in which ionic and ion-covalent bonding within the LnO and FeAs layers, respectively, is accompanied by the weak ionic bonding of these layers. The magnetic moments on Fe atoms calculated for AF2 are $1.56 \mu_B$ (Ln=La) and $1.33 \mu_B$ (Ln=Sm). These differ significantly from the values suggested by Mössbauer measurements ($\sim 0.35 \mu_B$) [23].

To find the energy barrier separating the fully relaxed AF2' and AF2'' configurations, we calculated the total energies $E_{AF2'}$ and $E_{AF2''}$ along the path ℓ_1 connecting \mathbf{O}_1 and \mathbf{O}_2 (inset in Fig. 2). Path ℓ_1 is parallel to the vector $\mathbf{n}=(1,-1)$ in the a - b plane. The $E_{AF2'}(Q)$ and

$E_{AF2''}(Q)$, where $Q=a-b$, are plotted in Fig. 2. For comparison, we also calculated $E_{AF1}(Q)$ along the path $\ell_2 \parallel \mathbf{n}$.

The calculated values of E_1 , E_2 , and E_3 are 0.005 eV, 0.025 eV, and 0.15 eV, respectively, for LaFeAsO and 0.006 eV, 0.026 eV and 0.11 eV for SmFeAsO . We note that approximate exchange-correlation functionals, such as PW91, can underestimate the values of energetic characteristics by as much as 100%. More reliable values of E_1 , E_2 , and E_3 , as well as those of Fe magnetic moments, can be obtained by applying methods, which include exact exchange interaction and allow for coupling of different many-electron states [24].

At $Q=0$, AF2' and AF2'' have the same atomic structures and $E_{AF2'}=E_{AF2''}$, yet, their electronic states are different. This situation leads to Jahn-Teller (JT) instability [25] and formation of a conical intersection at the crossover of the potential energy surfaces (PESs) $E_{AF2'}$ and $E_{AF2''}$. Correcting for non-adiabatic behavior near the intersection, together with taking into account the coupling of many-electron states, introduces an effective interaction V , which splits the $E_{AF2'}$ and $E_{AF2''}$ into a higher-energy single-well potential (E_S) and a lower-energy double-well potential (E_D) [25] as shown in Fig. 2. We can conservatively estimate that $0 < V < E_1$.

The lattice dynamics, described by E_S and E_D , has three regimes depending on the temperature (T):

1. For $T < E_1 - V$, the atoms vibrate near their positions defined by one of the orthorhombic energy minima of E_D (e.g. \mathbf{O}_1). In this case the magnetic structure is dominated by AF2' configuration (see Fig. 2).
2. For $E_1 - V < T < E_1 + V$, motion of atoms is determined by parabolic branches of E_D , although the effect of the barrier separating its energy minima can not be neglected. The difference between the average distribution of short and long Fe-Fe bonds decreases with increasing temperature, which corresponds to a gradual transition from O to T symmetry. Magnetic order is lost because the Fe spins adjust themselves to the momentary local atomic structure, so as the spins are parallel for Fe atoms forming short Fe-Fe bonds and anti-parallel otherwise. In other words, thermal fluctuations of Fe-Fe bond lengths cause reorientation of Fe spins (Fig. 2).
3. For $T > E_1 + V$, the lattice dynamics is determined by parabolic branches of E_S and E_D and the effect of the barrier in E_D can be neglected. The lattice has the T-symmetry. There is no magnetic order because the orientation of the spins changes according to the local atomic structure, as described in 2, and also due to coupling of electronic states of E_S and E_D .

Experimental observations of the structural and magnetic phase transitions in LaFeAsO (e.g. [10, 11, 26]) suggest that the T \rightarrow O transition takes place gradually, with the $Q=a-b$ order parameter exhibiting two kinks at T_{max} (~ 160 K) and T_{min} (~ 140 K), and that the magnetic phase transition occurs at T_{min} or slightly below it. In addition, specific heat capacity displays two peaks,

which also seem to coincide with T_{max} and T_{min} [11, 13]. Similar data have been reported for other FeAs-based materials [9]. These results are consistent with the model for the three regimes of the lattice dynamics outlined above, in which two phase transition temperatures T_{max} and T_{min} correspond to $E_1 + V$ and $E_1 - V$, respectively. We can also speculate, that the decrease in the amplitude of atomic vibrations during **T**→**O** transition [27] can contribute to the abrupt drop in the electrical resistivity observed, for example, in [1].

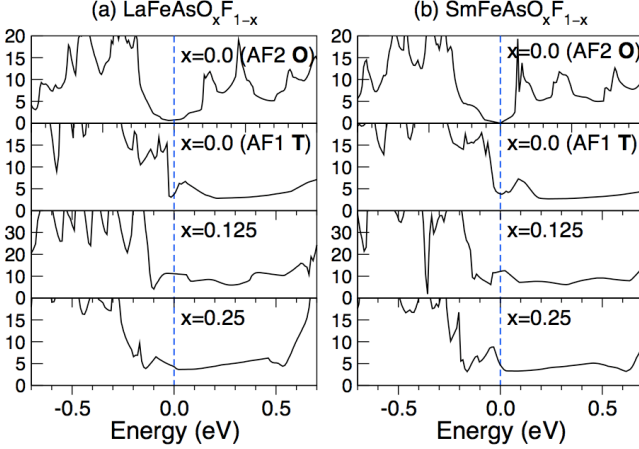


FIG. 3: Density of states for (La,Sm)FeAsO_xF_{1-x}. Letters **O** and **T** refer to the orthorhombic and tetragonal phases, respectively. The Fermi energy is at 0.0 eV.

We now consider the effect of F-doping on the atomic and electronic structures of LnFeAsO. The doping provides additional electrons to the FeAs layer so as the charge distribution becomes (LnO)^{+δ+x}(FeAs)^{-δ-x} and the lattice parameter c decreases due to the increased inter-layer ionic bonding (Table I). This leads to opening up of a narrow gap in the $N(\varepsilon)$ at ~ 2.5 eV below the ε_F (not shown).

We find that the spin-density distribution in the FeAs layers is not independent on the arrangement of the F impurities. For example, for $x=0.25$ ($\sqrt{2} \times \sqrt{2}$ cell), the spin-down density is localized on a single Fe atom nearest to the F⁻ impurity, while the remaining three Fe atoms share the spin-up density. At the doping level of $x=0.125$ (2×2 cell), the effect is more subtle. The lowest energy state is similar to that of the undoped LnFeAsO: the lattice structure corresponds to **O**-symmetry of the $\sqrt{2} \times \sqrt{2}$ cell and the spin-arrangement is the same as in AF2, although the values of μ_{Fe} are reduced to 1.32 (Ln=La) and 0.75 μ_B (Ln=Sm). We also found a spin-disordered state, which has the **T**-symmetry and is ~ 7 (Ln=La) and ~ 5 (Ln=Sm) meV per Fe atom higher than the ground state. Taking into account the generally random distribution of the F impurities over O lattice sites in realistic samples, we suggest that such spin-disordered state realizes in practice.

For $x=0.125$ (2×2 cell) we distinguish two sets of non-equivalent Ln and As atoms with different values of their z -coordinates. The effect of such structure on the lattice phonons and on the charge- and spin-density distributions needs to be considered separately.

Finally, we investigate the correlation between the structure and doping level and the electronic density of states $N(\varepsilon)$ calculated for the fully relaxed AF1, AF2, and doped LnFeAsO_{1-x}F_x (Fig. 3). In all cases the $N(\varepsilon)$ near the Fermi energy (ε_F) is dominated by the Fe 3d states and the polarization of spin-up and spin-down states is negligible.

In stoichiometric LnFeAsO, $N_{AF2}(\varepsilon)$ has a pronounced depression near ε_F , while the $N_{AF1}(\varepsilon)$ has a narrow deep minimum separating a steep rise at $\varepsilon < \varepsilon_F$ and a peak at $\varepsilon > \varepsilon_F$ [28]. Projecting $N_{AF1}(\varepsilon)$ on the d -states shows that this peak is dominated by d_{xz} and d_{yz} states. The same $d_{xz}+d_{yz}$ peaks near ε_F are evident for the doped LnFeAsO (Fig. 3).

TABLE I: Structural parameters of LnFeAsO_{1-x}F_x (Ln=La,Sm). In all cases crystallographic cell angles α , β , and γ deviate from 90° by less than 0.0005°. Letters E and T refer to experiment and theory (this work) respectively.

x	details	a , Å	b , Å	c , Å	$z(\text{Ln})$	$z(\text{As})$
LaFeAsO _{1-x} F _x						
0.0	AF1 T	5.6873	5.6899	8.6185	0.1448	0.6383
0.0	AF2 T	5.7305	5.6672	8.6948	0.1433	0.6438
0.0	300 K E [10]	5.7031	5.7031	8.74111	0.1413	0.6517
0.0	120 K E [10]	5.6826	5.7104	8.71964	0.1417	0.6513
0.125	T	5.6829	5.6829	8.5630	0.1560	0.6405
					0.1452	0.6394
0.25	T	5.6873	5.6831	8.4859	0.1562	0.6410
0.14	120 K E [10]	5.6844	5.6844	8.6653	0.1477	0.6527
SmFeAsO _{1-x} F _x						
0.0	AF1 T	5.5955	5.5918	8.3435	0.1406	0.6472
0.0	AF2 T	5.6232	5.5623	8.4142	0.1396	0.6515
0.125	T	5.5834	5.5834	8.2884	0.1523	0.6496
					0.1413	0.6479
0.25	T	5.5888	5.5902	8.2046	0.1529	0.6493

According to the standard BCS theory of superconductivity, the transition temperature T_c is proportional to $\langle \omega \rangle \exp[-1/\lambda N(\varepsilon_F)]$, where $\langle \omega \rangle$ is a typical phonon frequency and λ is the electron-phonon coupling constant. As shown in Ref. [29], the limitation of $T_c < 40$ K, suggested by Migdal's theorem for BCS superconductors, is not justified and, therefore, much higher values of the T_c can be achieved by optimizing $\langle \omega \rangle$, λ , and $N(\varepsilon_F)$. We can tentatively suggest that $\langle \omega \rangle$ and λ do not vary strongly for FeAs-based compounds, since the conductivity is confined to the FeAs layers. Then T_c can be considered as a function of a single parameter $N(\varepsilon_F)$.

Thus, we consider the correlation between the behavior of $N(\varepsilon)$ for ε close to ε_F (Fig. 3) and experimentally observed properties of $\text{LnFeAsO}_{1-x}\text{F}_x$ superconductors. First, we notice that as x increases and ε_F shifts across the $d_{xz}+d_{yz}$ peak, the value of $N(\varepsilon_F)$ increases as well, then reaches its maximum and then decreases. The details of the peak structure depend of the value of x but its general shape is reminiscent of the experimentally observed dependence of the T_c on x (e.g. [1, 12]).

Furthermore, the maximum of the $d_{xz}+d_{yz}$ peak ($x=0.0$) in SmFeAsO is higher and further away from ε_F than that in LaFeAsO . This correlates with the observations that the optimal T_c is higher in $\text{SmFeAsO}_{1-x}\text{F}_x$ (46 K, $x=0.15$ [5]) than in $\text{LaFeAsO}_{1-x}\text{F}_x$ (26 K, $x=0.05-0.12$ [1]) and that it is achieved at larger values of x . The slope of $N(\varepsilon_F)$ calculated for $x=0.125$ is negative for $\text{Ln}=\text{La}$ and positive for $\text{Ln}=\text{Sm}$, which indicates that maximum of $N(\varepsilon_F)$ can be found at $x < 0.125$ for $\text{Ln}=\text{La}$ and $x > 0.125$ for $\text{Ln}=\text{Sm}$. This is consistent with the optimal values of x found for these compounds as ~ 0.11 ($\text{Ln}=\text{La}$) [1] and ~ 0.20 ($\text{Ln}=\text{Sm}$) [12].

Finally, we notice that the $d_{xz}+d_{yz}$ peak in LaFeAsO is wider than that in SmFeAsO (this is clearly seen for $x=0.0$ and 0.125), which suggests that T_c has a stronger dependence on x in SmFeAsO as observed in [12]. While these observations say little about the mechanism of the superconductivity in FeAs-based materials, they suggest that the highest T_c can be achieved in those, which have the largest magnitude of the $d_{xz}+d_{yz}$ peak close to ε_F .

To summarize, we investigated the PESs for different magnetic states of stoichiometric LnFeAsO ($\text{Ln}=\text{La}, \text{Sm}$) and found that the properties of this system are determined by two close-lying PESs: a lower-energy double-well potential, where each well corresponds to the orthorhombic symmetry, and a higher-energy single-well potential of the tetragonal symmetry. This complex potential energy surface gives rise to three temperature ranges, and, therefore, two transition temperatures, and can explain the experimentally observed structural phase transition, the appearance of the magnetic order, and the anomaly in the temperature dependence of the specific heat capacity.

We noticed a correlation between the calculated profile of $N(\varepsilon)$ near ε_F and experimentally observed dependence of the T_c on the dopant concentration x and on the type of Ln atom. This correlation can be used for computational prescreening of the promising LnFeAsO derivatives as well as for predicting optimal dopant concentrations via relatively inexpensive electronic structure calculations.

The authors thank C. Rüegg and A. M. Stoneham for their comments on the manuscript and S. W. Kim, Y. Kamihara, T. Nomura, and T. Kamiya for valuable discussions. P. V. S. is grateful to Japan Science Foundation and WPI-AIMR at Tohoku University. The access to HPCx is provided via the Materials Chemistry Con-

sortium.

-
- * Corresponding author. Email address: p.sushko@ucl.ac.uk
- [1] Y. Kamihara, T. Watanabe, M. Hirano, and H. Hosono, *J. Am. Chem. Soc.* **130**, 3296 (2008).
 - [2] J. G. Bednorz and K. A. Müller, *Z. Phys.* **B64**, 189 (1986).
 - [3] Y. Kamihara, H. Hiramatsu, M. Hirano, R. Kawamura, H. Yanagi, T. Kamiya, and H. Hosono, *J. Am. Chem. Soc.* **128**, 10012 (2006).
 - [4] T. Watanabe, H. Yanagi, T. Kamiya, Y. Kamihara, H. Hiramatsu, M. Hirano, and H. Hosono, *Inorg. Chem.* **46**, 7719 (2007).
 - [5] X. H. Chen, T. Wu, G. Wu, R. H. Liu, H. Chen, and D. F. Fang, *Nature* **453**, 761 (2008).
 - [6] H. Takahashi, K. Igawa, K. Arii, Y. Kamihara, M. Hirano, and H. Hosono, *Nature* **453**, 376 (2008).
 - [7] J. Yang, Z.-C. Li, W. Lu, W. Yi, X.-L. Shen, Z.-A. Ren, G.-C. Che, X.-L. Dong, L.-L. Sun, F. Zhou, et al., *Supercond. Sci. Technol.* **21**, 082001 (2008).
 - [8] P. M. Grant, *Nature* **453** (2008).
 - [9] M. Rotter *et al.*, cond-mat/0805.4021.
 - [10] T. Nomura *et al.*, cond-mat/0804.3569.
 - [11] M. A. McGuire *et al.*, cond-mat/0806.3878.
 - [12] S. Margadonna *et al.*, cond-mat/0806.3962.
 - [13] Y. Kohama *et al.*, cond-mat/0806.3304.
 - [14] K. Haule, J. H. Shim, and G. Kotliar, *Phys. Rev. Lett.* **100**, 226402 (2008).
 - [15] D. J. Singh and M.-H. Du, *Phys. Rev. Lett.* **100**, 237003 (2008).
 - [16] S. Ishibashi, K. Terakura, and H. Hosono, *J. Phys. Soc. Jpn.* **77**, 053709 (2008).
 - [17] I. I. Mazin *et al.*, cond-mat/0803.2740.
 - [18] K. Kuroki *et al.*, cond-mat/0803.3325.
 - [19] T. Yildirim, cond-mat/0804.2252.
 - [20] J. P. Perdew and Y. Wang, *Phys. Rev. B* **46**, 12947 (1992).
 - [21] P. E. Blöchl, *Phys. Rev. B* **50**, 17953 (1994).
 - [22] G. Kresse and J. Furthmüller, *Phys. Rev. B* **54**, 11169 (1996).
 - [23] S. Kitao *et al.*, cond-mat/0805.0041.
 - [24] L. Hozoi and M. S. Laad, *Phys. Rev. Lett.* **99**, 256404 (2007).
 - [25] A. M. Stoneham, *Theory of Defects in Solids*, vol. 1 (Clarendon Press, Oxford, 1975).
 - [26] C. de la Cruz, Q. Huang, J. W. Lynn, J. Li, W. R. II, J. L. Zarestky, H. A. Mook, G. F. Chen, J. L. Luo, N. L. Wang, et al., *Nature* **453**, 899 (2008).
 - [27] J. M. Ziman, *Principles of the theory of solids* (Cambridge University Press, Cambridge, 1972).
 - [28] $N_{AF2}(\varepsilon)$ in the **T**-phase (not shown) and **O**-phase differ slightly near ε_F in that $N_{AF2}(\varepsilon_F)$ decreases and $N_{AF2}(\varepsilon)$ elsewhere in the ~ 0.2 eV vicinity of ε_F increases as a result of the **T**→**O** transition, which can be interpreted as the effect of the JT distortion. However, this effect is much smaller than the difference between $N_{AF2}(\varepsilon)$ and $N_{AF1}(\varepsilon)$.
 - [29] A. A. Abrikosov, *Physica C* **468**, 97 (2008).